

2

Electrochemical nanobiomemory devices: Recent developments and future challenges

Ajay Kumar Yagati^{1,2} and Jeong-Woo Choi^{1,3,*}

¹Interdisciplinary Program of Integrated Biotechnology, Sogang University, Seoul, 121-742, Republic of Korea

²Department of Biomedical Engineering, Gachon University, Yeonsu-gu, Incheon 406-799, Republic of Korea

³Department of Chemical and Biomolecular Engineering, Sogang University, Seoul, 121-742, Republic of Korea

*Corresponding author

Outline:

Introduction.....	24
<i>Challenges in biomemory device technology.....</i>	24
<i>Role of nanotechnology in the development of biomemory device.....</i>	25
Biomemory based on electrochemical switching.....	26
<i>Mechanism of memory switching: Electrochemical charge transfer at the electrode.....</i>	26
<i>Time dependent charge and current measurements.....</i>	27
Recent developments for biomemory applications.....	28
<i>Memory performance enhancement.....</i>	28
<i>Design of Au nano pattern electrodes using mask and template synthesis.....</i>	28
<i>Design of Au nano pattern electrodes using nanosphere lithography technique.....</i>	29
<i>Multi-bit storage capacity of biomemory device.....</i>	30
<i>Multi-level storage based biomemory device.....</i>	32
<i>Design of hybrid biomaterials.....</i>	35
New concepts for advanced biomemory devices.....	36
<i>Novel hybrid biomaterials higher storage density and information processing.....</i>	36
<i>Single molecular and solid state biomemory devices.....</i>	38
Conclusions.....	42
Acknowledgements.....	43
References.....	43

Introduction

The performance of the integrated circuits has shown an exponential growth since the last two decades but the reduction in device size still remains as the main goal since the invention of the first junction transistor. The integration of high density devices allowed the growth of memory size and clock frequency, which had a strong impact on economy. Therefore, many engineers and scientists have been working for years on scaling the devices to achieve micro/nano-scale architectures. However, as the size of the structures has been reduced, the complexity and cost of fabrication have increased exponentially. Basically, the continuity of this miniaturization trend is becoming difficult due to the limitations of conventional lithography, complexity of integration, physical phenomena [1].

On the other hand, nature has already perfectly controlled and manipulated nano-scale components using molecular recognition of various biological materials such as deoxyribonucleic acid (DNA), protein, bacteria and cell. Therefore, mimicking or exploiting the behaviour of biomolecules can be used to solve the problems of miniaturization. Recently many researchers have applied this knowledge to develop artificial nano/microstructures towards bioelectronic devices [2,3]. Additionally, genetic engineering and chemical methods can optimize the binding, catalytic and electron transport properties that enable to integrate biomaterials with electronic elements to develop functional biodevices. Therefore, biomaterials such as protein and DNA due to its size and electronic properties could be a next alternative to succeed the silicon based technologies in developing novel electronic devices [4].

With these strategies, a bioluminescent molecular switch for glucose was developed by insertion of glucose binding protein (GBP) into the structure of the photoprotein aequorin (AEQ) [5]. In the presence of glucose, GBP undergoes a conformational change, bringing the two segments of AEQ together, “turning on” bioluminescence and detecting glucose. Also, a photonic DNA based memory device was developed which utilizes positional information of DNA for scaling up the address space in DNA based memory device. This optical based technique was useful for parallel processing of data by controlling the positional addresses [6]. Further, multiple logic gates based on electrically wired surface-reconstituted enzymes, and multifunctional logic gate based on folding/unfolding transitions in a protein was reported [7,8]. Also, protein patterns on solid surface by a lithography technique was explained to perform *write*, *read* and *erase* operations [9]. A two layered dielectric film comprises of a self-assembled monolayer (SAM) and an electrolyte was exploited to study and to control the capacitance and electromotive force through a redox reaction between the SAM and the electrolyte [10]. Furthermore, virus conjugated with nanoparticles also exhibited bi-stable charge storage states in their conductance measurements to develop non-volatile memory devices [11]. Recently, redox properties of a genetically engineered recombinant metalloprotein were utilized as a charge storage element to demonstrate a protein based biomemory device [12].

Challenges in biomemory device technology

For decades, semiconductor technology has advanced at an exponential rate as described by Moore’s law, which states that the number of features in a given area of substrate doubles at every 2 years shown in Figure 2.1. As a result of Moore’s law, the computing power and capabilities were increased with each generation of device while the cost per function was decreased. A relentless decrease in the size of silicon-based microelectronics faces the problems imposed by quantum-size effects and instabilities introduced by the effects of thermal fluctuations. These problems

prompted researchers to focus on the use of biomolecules as they have the advantages of functionality and specificity. Much work has been done in the bioelectronics field since the 1990s has been focused on creating better bioelectronic devices by integrating biomolecules with semiconductors [13]. Although advances have been made in binding biological molecules to substrates, but bioelectronics faces important challenges for the future. The development of high throughput electronic detection assays in chips, the development of miniaturized implantable sensor or machinery devices for controlled drug release and prosthetic activation, and the assembly of complex biomaterial-based metal/semiconductor circuitry with signal processing capabilities represent some of these goals. It is anticipated that bioelectronics will provide exciting opportunities for interdisciplinary research of chemists, physicists, biologists and material scientists.

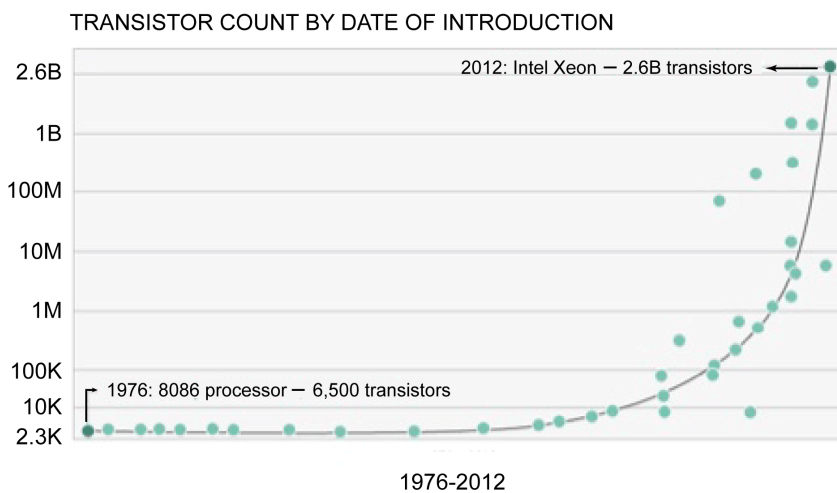


FIGURE 2.1

Moore's law indicating the number of transistors on Intel processors have doubled approximately every two years

One of the major obstacle in the area of bioelectronics is the lack of electrical communication between the biomaterial components and the electronic elements. Electrical communication which is essential for the functional operation of the bioelectronic systems is accomplished by the nanoengineering of biomaterials by chemical methods and the immobilization of biomaterials on surfaces in tailored, predesigned architectures. Thus, with the advancement of nanotechnology, the inter connection between the biomaterial with other nanomaterials to the underlying electrode is apparently possible. Yet again, the major problem in developing protein based storage device is the stability, durability, operating conditions and the non-volatile nature. These issues needs to be addressed in order to compete with the present silicon based technologies. The present chapter highlights these issues along with recent developments in protein based biomemory devices.

Role of nanotechnology in the development of biomemory device

The integration of biomolecules with electronic elements, due to their nanometer size and inherent properties, has shown many advances in the field of bioelectronics. The role of nanotechnological tools should be able to produce electronic devices and circuits with smaller dimensions, faster

processing times, and cheaper production costs. Further, new capabilities enabled through chemical methods of nanofabrication that results in creation of nanoscale chemical patterns. Hence several researchers proposed different kinds of methodologies to develop nanoscale electronic devices. Both bio and nanotechnologies provide new and unique opportunities and allow researchers to exploit key and tunable properties of bionanomaterial that go far beyond the capabilities of conventional fabricated electronics in building highly sophisticated and multifunctional bioelectronic interfaces [14].

However, a smooth transition from micro to nano, or the smooth integration of nanotechnology with conventional technologies, is essential. The two facets of nanotechnology can be explained by, *evolutionary nano* which is represented by the steady miniaturization of Si based devices using the top-down method, whereas *revolutionary nano* indicates miniaturization using bottom-up method. Although revolutionary nano attracts widely and thus much research is focused in this field, however, evolutionary nano is mainly contributes to the industry [15]. To successfully commercialize the revolutionary nano, it should demonstrate many technological innovations and at the same time much research should be focused on evolutionary nano, which should be united with revolutionary nano. Both playing a synergic effect in the development of nanotechnological materials.

Biomemory based on electrochemical switching

Mechanism of memory switching: Electrochemical charge transfer at the electrode

Electrochemical properties of redox proteins, whose redox states can be controlled by external voltage, are of the fundamental and practical importance in many bioelectrochemical applications. These redox properties are often depending on the biochemical activity of transition metal ions as cofactors within the active sites of proteins. For potential utilization of redox-active protein monolayers as a molecular-scale information storage device, a direct electrical communication with the underlying electrode is often necessary. This can be achieved by site directed mutagenesis (SDM) method by introducing cysteine residues in metalloprotein to directly coordinate with the Au surface. The molecules generated with recombinant technology have the capability to adsorb on bulk Au as well as nanosize Au electrodes without the use of any additional linker materials. Furthermore, the redox properties of protein on conducting electrode can be examined through cyclic voltammetry (Figure 2.2a). These voltages can be utilized is performing the biomemory functions. Hence, the operating principles of biomemory using redox metalloprotein can be explained as, application of oxidation potential causes transfer of electrons from the protein self-assembled monolayer (SAM) to the underlying Au substrate, resulting in storage (“write”) of positive charges in protein SAM. On contrary, application of reduction potential causes transfers of electrons back into the protein SAM, thereby “erasing” the stored charge. These two states of the protein layer were “read” by the equilibrium potential or open circuit potential (OCP) to successfully realize a biomolecular device (Figure 2.2b).

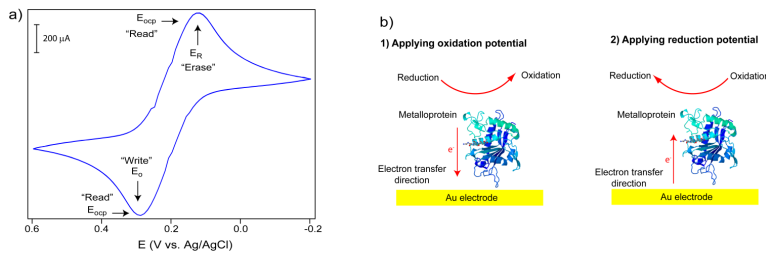


FIGURE 2.2

Schematic diagram shows the electron transfer mechanism of a recombinant ferredoxin on Au electrode. (a): Application of oxidation voltage causes the electron to move from the protein to Au electrode. (b): Application of reduction voltage caused the electron back to the protein. Schematics drawn are not to scale

Time dependent charge and current measurements

The measurements of the faradaic currents for validating the memory switching performance can be performed with an electrochemical analyzer in three electrode system. As shown in Figure 2.3, *Rhodobacter sphaeroides* ferredoxin (fdx) was covalently adsorbed on Au surface without any chemical linkers. This is possible by incorporating cysteine residues in protein by site directed mutagenesis method which avoids usage of any additional linkers and allows direct attachment to Au surface. The cyclic voltammetry of fdx on Au electrode when scanned in a potential range of -0.1 to -0.7 V vs. Ag/AgCl at a scan rate of 50 mV/s revealed a cathodic peak at -0.5 V and anodic peak at -0.26 respectively and the open circuit measurements found to be -0.2 V. Information about the reduction and oxidation of the protein molecules can be obtained from the measurement of OCP with time. For measuring the OCP, protein immobilized Au surface was made as working electrode with Platinum wire and Ag/AgCl electrodes were used as counter and reference electrode in the electrochemical experiment. The potential decay in solution in open circuit conditions with time has been recorded. Prior to any amperometric measurements the cell was disconnected for some time so that the cell reaches to OCP. These three voltages (oxidation, reduction and OCP) can be utilized to charge storage, erase and read functions.

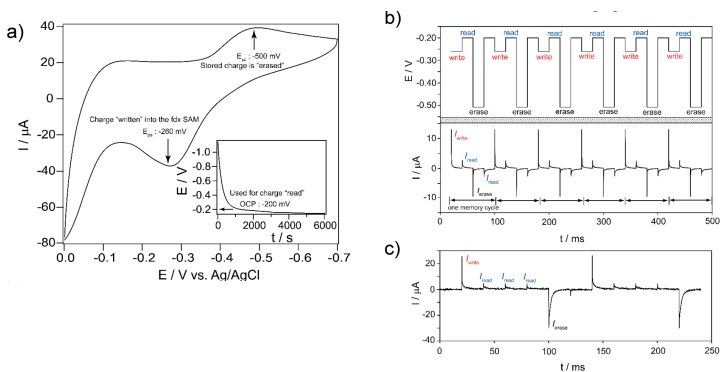


FIGURE 2.3

a) Cyclic voltammogram for ferredoxin immobilized Au electrode in 10 mM Tris-HCl buffer with pH 7.4 at a scan rate of 50 mV/s. Shown in inset is the open circuit potential for ferredoxin immobilized Au electrode, b) Write-read-erase cycles of a protein based biomemory device. The top curve shows the applied sequence of pulses for "write" "read" and "erase" functions and the bottom curve is corresponding current response. Figure reproduced with permission from: ref. 16, © 2019 Elsevier

The charge densities can be obtained from chronoamperometric (CA) measurements and the magnitude of the charge measured was found to be decreased as a function of time. The current or charge can be measured with Cottrell's equation during the time represents the total charge retained in the protein SAM. Faradaic currents were measured by CA of oxidized protein on Au electrode where charging currents were measured by changing the disconnecting time which is the interval between the oxidation of the self-assembled monolayer (SAM) and subsequent reduction of SAM at OCP. The charge-retention half-life represents the kinetics of charge recombination of the oxidized SAM with electrons in the working electrode surface. Charge retention information can be obtained through integration of the charging current transients. These charge densities were obtained from the instantaneous current measured during CA. Figure 2.3(b,c) show the chronoamperometric measurements observed for memory functions operations along with multiple *read* operations in a protein based memory device.

Recent developments for biomemory applications

Memory performance enhancement

The strategy to increase memory density inflicts a multi-bit and multi-level approach wherein the charge storage element contains molecules with multiple redox states. To demonstrate this approach, the redox molecule is adsorbed on multi electrode system subsequently the charge information is obtained. Also, by mixing different redox protein molecules higher memory densities can be achieved. Therefore, in order to achieve memory function with increased memory density, nano-sized electrode are necessary and also multiple redox molecular systems such as proteins are required.

Design of Au nano pattern electrodes using mask and template synthesis

Aluminum oxide layer was prepared from an aluminum foil (99.99%, 100 μm thickness) by a two-step anodization method which has been reported elsewhere [17]. An aluminum foil was achieved by the pretreatment of electro-polishing in a mixed solution of perchloric acid and ethanol (1:4 in volume) for 60 s. First anodization of Al electrode was performed by applying a constant DC voltage of 40 V in 0.3 M oxalic acid solution of 3 $^{\circ}\text{C}$ for 8 h. After the first anodization, the generated anodic aluminum oxide (AAO) was removed by immersing the sample in a 60 $^{\circ}\text{C}$ solution composed of a mixture of phosphoric acid (1.8 wt%) and chromic acid (2 wt%). Then the second anodization was carried out under the identical conditions for 5 min. The thickness of AAO formed by anodization for 5 min is below 500 nm. After the second anodization, the remaining aluminum substrate was removed in a saturated HgCl_2 solution. After the lift-off process, the barrier layer at the bottom of the AAO was uniformly etched out in an aqueous 5 w% phosphoric acid at 30 $^{\circ}\text{C}$, sequentially. In this process, to remove thoroughly the barrier layer of AAO is very important for fabrication of the AAO mask with through-hole. Then the AAO mask with through-hole was placed onto ITO substrate for fabrication of Au nanodots. Then pure gold was deposited by thermal evaporation at a vacuum pressure of 1×10^{-6} Torr. After Au deposition, the AAO mask was dissolved in 1 M NaOH solution for several minutes and then rinsed with distilled water. The Au nanodots formed on ITO substrate revealed after removal of the AAO mask. Finally, azurin protein was allowed to adsorb on the nanoscaled electrode to store information on each Au-dot using electrochemical scanning

tunneling microscopy (ECSTM) under bipotentiostic control to exploit the memory function mechanism.



FIGURE 2.4

Schematic diagram showing the fabrication of Au nanodots arrays on ITO surface by AAO mask and protein immobilization on the patterned Au dots

Design of Au nano pattern electrodes using nanosphere lithography technique

Nanosphere lithography is one of the simplest and yet effective to produce nano electrodes over a large area [18]. To achieve this masks were created by spin-coating polystyrene nano-spheres on the cleaned ITO substrates by a spin coater. Particles of $0.46\ \mu\text{m}$ were spin-coated at a speed of 2000 rpm for 20 sec. The physical dimensions of the substrate were chosen to be $1.0\ \text{cm}^2$, where the entire substrate surface was spin-coated with nano-spheres. The nano-spheres were received from the company as 10 wt% dispersion in water and then further diluted in a solution of the surfactant Triton X-100/methanol (1:400 by volume) before spin-coating. The dilution factors for single-layer masks were ca. 1:1 (by volume) for 460 nm particles. The surfactant was used to assist the solutions in wetting the substrate. Double-layer masks were self-assembled by increasing the nanosphere concentration and dilution factors in the spin-coating solution to optimize the double layer surface coverage. Thin films of Au were deposited through vacuum evaporation over the modified substrates. To reveal the patterned dot arrays, the polystyrene spheres “lift off” from the ITO substrate by dissolution in methylene chloride (CH_2Cl_2) with the aid of sonication for 1~2 min. These electrodes can also be exploited to utilize various bioelectronics applications [19].

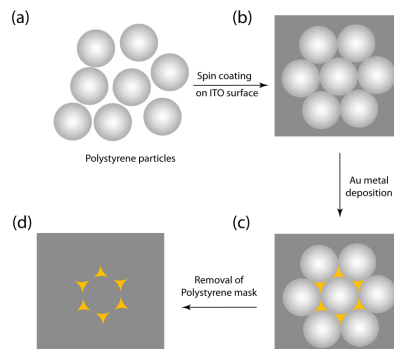


FIGURE 2.5

Schematic drawings of the fabrication of Au nanopattern array on a ITO substrate nanosphere lithography (NSL): (a) A mono layer colloidal crystal of polystyrene particles were spin coated on the ITO substrate, (b) The template is top-coated with Au metal by physical vapor deposition by which some of the Au deposited penetrates through the interstices and down onto the substrate, (c) The template is removed, leaving only the material deposited on the substrate, (d) the Au pattern after the removal of the polystyrene mask. Figure reproduced with permission from: ref. 19, © 2013 Elsevier

Multi-bit storage capacity of biomemory device

Here, an efficient way of Azurin (a redox protein with *Cu* metal center) thin film formation on Au electrodes is introduced which will act as a memory element to achieve the basic memory function with multiple bit storage capacity. Azurin possesses two distinct electrochemical states (oxidation and reduction states) which can be controlled by applied potential. Azurin is recombined with a cysteine residue by site-directed mutagenesis and immobilized directly on 4 different Au electrodes to store 16 different data and their read-out. This direct immobilization can enhance the efficiency of electron transfer between azurin layer and Au surface by a well oriented protein structure using Au-S bond without any chemical linker, which allows a unidirectional electron flow from the protein to gold surface. The memory function of the proposed device was carried out by electrochemical methods on the multibit electrode system.

Using the proposed biomemory device, the enhancement to store multiple bits in the device was performed by applying potentials of oxidation, reduction and OCP to all four Au electrodes. The multi-bit biomemory device was verified by monitoring the faradaic currents upon applying the input potentials. Input voltage pulses of oxidation and open circuit potential were applied to the four Au electrodes for the duration of 25 ms consisting azurin SAM and corresponding charging currents were measured as shown in Figure 2.6(a). In experiment 1, when the electrodes no. 1 and 3 were applied with oxidizing potential, it produces a high faradaic current nearly 7 μA whereas the electrodes no. 2 and 4 were connected with OCP produces practically a low current of 2 μA . In the proposed device, the low faradaic current indicates storage of bit "0" and high faradaic currents indicates storage of bit "1" as shown in the truth table. Hence a logic pattern of 1010 can be stored in the biodevice as shown in the table Figure 2.6(b).

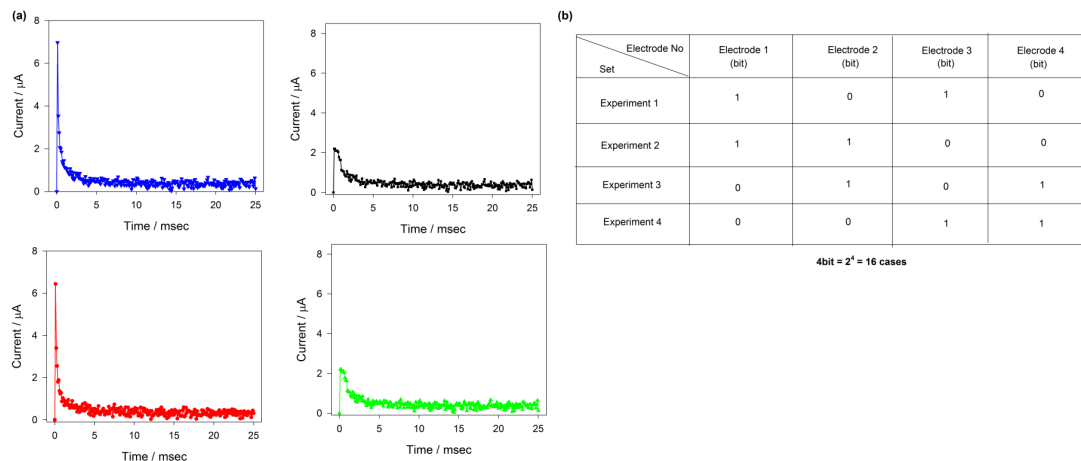


FIGURE 2.6

Faradaic currents observed from a four-bit memory device. (a) Application of oxidation and open circuit potentials in tandem to the four electrodes (high current represents storage of "1" and low current represents "0") represents a 1010 logic system and (b) table represents the results obtained from 4 experiments for storing bits by these combinations similarly this can be extended for all 16 combinations. Figure reproduced with permission from: ref. 20, © 2009 Elsevier

Similarly, experiments for four different combinations of input bias potentials were applied to the electrodes and corresponding faradaic currents were measured as shown in the table. In this

manner, input potentials with 16 different combinations can be applied and each provides a combination of logical patterns. Finally, it is concluded that the proposed bioelectric device composed of azurin layer can be used as multi-bit molecular storage system by controlling the redox potentials of azurin.

Another technique to increase the memory density, in which cysteine-modified azurin was designed using the site directed mutagenesis method (SDM) with 4 different metal centers were introduced to make a 4-bit biomemory chip that could perform multi-functions. A recombinant protein containing a cysteine residue and different metal substitutes was designed and directly immobilized on an Au surface without any chemical linkers. The redox property of 4 different types of azurin (Co-substitutes type; Ni-substitutes type; Fe-substitutes type; Mn-substitutes type) variants were measured.

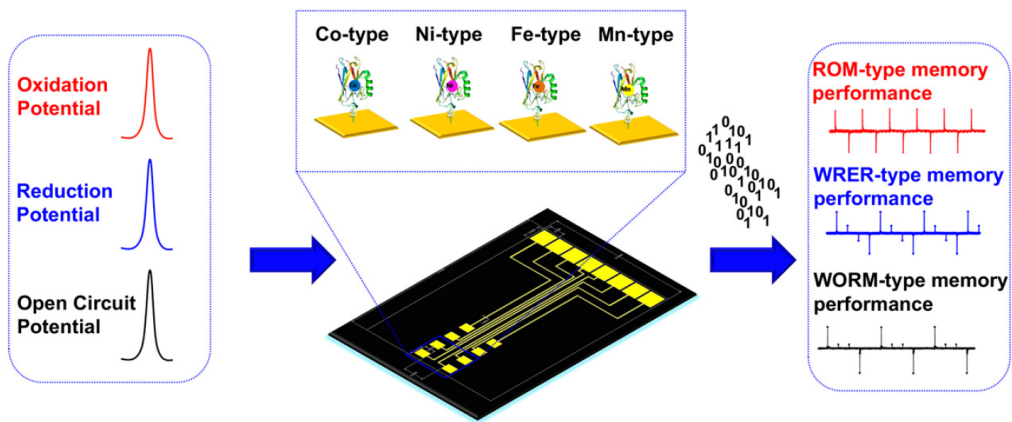


FIGURE 2.7

Schematic diagram of the basic operating mechanism of the fabricated biomemory chip. Figure reproduced with permission from: ref. 21, © 2011 Elsevier

Earlier sections it was discussed that the direct immobilized azurin variants layers have three distinct conducting states. Briefly, in the case of the Co-type azurin, applying of an oxidation potential (OP: 210.03 mV) resulted in the transfer of electrons from the immobilized azurin layer into the Au substrate, and positive charges were stored in the azurin layer. The opposite process occurred during the reduction step. When the reduction potential (RP: 74.10 mV) was applied, the electrons were transferred back into the azurin layer and the stored charge was erased. The OCP (182.11 mV) was then used to read these charged states. Fig. 2.8b shows the WRER-type memory behavior according to the applied potential for the Ni-type Azurin. In this case, the memory parameter of the Ni-type azurin was as follows; OP: 172.90 mV, OCP: 121.42 mV, RP: 51.60 mV. In the case of Fe-type azurin (OP: 236.09 mV, OCP: 154.76 mV, RP: 105.12 mV), the other functions were performed for WORM-type memory. An OP of 236.09 mV could reproducibly charge the device. A continuous set of two OCP pulses of 154.76 mV with small disconnecting times produced the necessary current responses and these charges maintained the oxidized state of the memory device. Finally, a RP pulse of 51.60 mV erased all of the stored charge. Fig.2.8c shows the basic mechanism of WORM-type memory performance.

The Mn-type azurin (OP: 132.61 mV, OCP: 104.26 mV, RP: 24.97 mV) also displayed a WORM-type current response with three defined parameters. In this case, when an OCP of 121.42 mV was

applied at very small disconnecting time to read the stored information 3 times, the observed current responses of the stored charge could be read 3 times. These results are shown in Fig. 2.8 (c, d) respectively. Overall, each azurin variant of the W-R-E-R full cycles and W-O-R-M full cycles could be reliably operated at the given potentials. To perform multi-functional biomemory behavior, the different given potentials were applied to each azurin variants-immobilized biomemory chip.

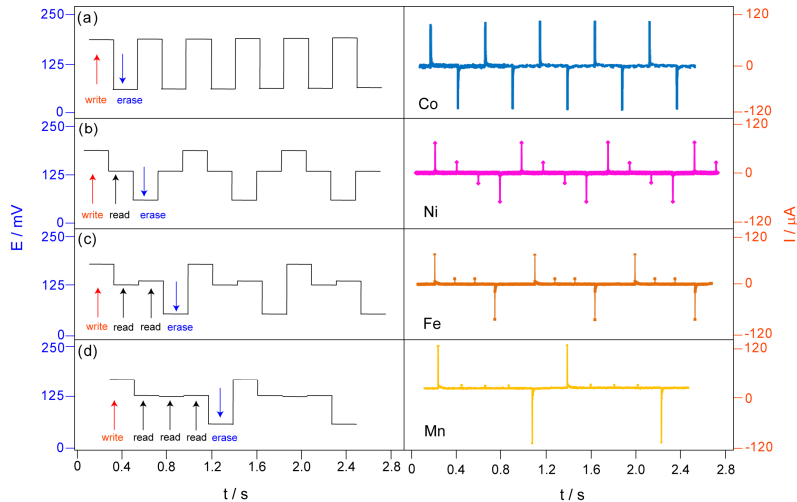
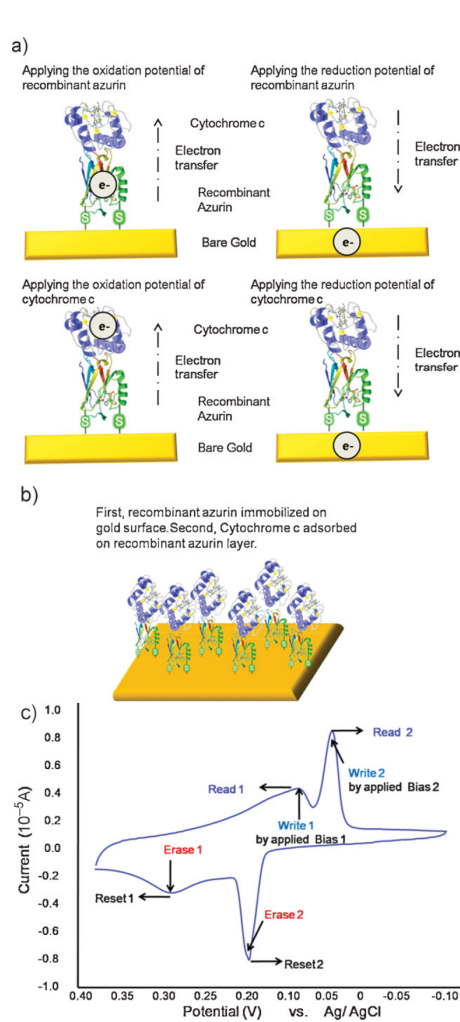


FIGURE 2.8

Verification of multi-functional memory performance of the (a) Co-type azurin (b) Ni-type azurin (c) Fe-type azurin (d) Mn-type azurin. The left part of the figure shows the applied potential where the OP and OCP, RP were assigned to the 'write', 'read' and 'erase' respective. The right part of figure displays the corresponding charging currents that were observed for a total duration of 2.8 s. Figure reproduced with permission from: ref. 21, © 2011 Elsevier

Multi-level storage based biomemory device

For multi-level storage, at first recombinant azurin containing cysteine residues was produced by site-directed mutagenesis and immobilized directly on an Au surface; then, cytochrome c was adsorbed onto the immobilized azurin layer by electrostatic bonding. This direct immobilization enhanced the efficiency of electron transfer between the azurin layer and Au surface and between the cytochrome c layer and Au surface due to the well-oriented protein structure, which resulted from using the Au-S bond without any chemical linker. In addition, this immobilization strategy allowed for a unidirectional electron flow from the protein to the Au surface. This heterolayer, composed of recombinant azurin and cytochrome c, was capable of storing the two pairs of information, which is referred to as the multi-state memory. Figure 2.9(a) shows a schematic diagram for the electron transfer mechanism between cytochrome c/recombinant azurin layer and Au surface, while Figure 2.9(b) shows a schematic diagram for the fabrication of a recombinant azurin/cytochrome c heterolayer. This multistate memory displayed two pairs of nonvolatile *write*, *read*, and *erase* functions (Fig. 2.9c).

**FIGURE 2.9**

a) The electron-transfer mechanism of a cytochrome *c*/recombinant azurin layer on an Au surface. b) Schematic diagram of protein immobilization, recombinant azurin immobilized onto gold surface, and then, cytochrome *c* adsorbed on the self-assembled azurin layer by electrostatic interactions. c) Schematic representation of a cyclic voltammogram for heterolayers that consist of recombinant azurin/cytochrome *c* on a gold surface; the memory function upon each application of a proper bias potential is depicted Figure reproduced with permission from: ref. 22, © 2010 WILEY-VCH

Cyclic voltammetry of the recombinant azurin/cytochrome *c* heterolayer immobilized on the Au surface shows two anodic waves at E_{pa} of 0.062 V vs. Ag/AgCl and cathodic wave at E_{pc} of 0.184 V vs. Ag/AgCl, which corresponds to the redox process of recombinant azurin center $Cu^{2+/1+}$. In addition, the anodic wave at E_{pa} of 0.131 V vs. Ag/AgCl and cathodic wave at E_{pc} of 0.324 V vs. Ag/AgCl was observed, which corresponds to the redox process of the cytochrome *c* center $Fe^{3+/2+}$ as shown in Figure 2.10a.

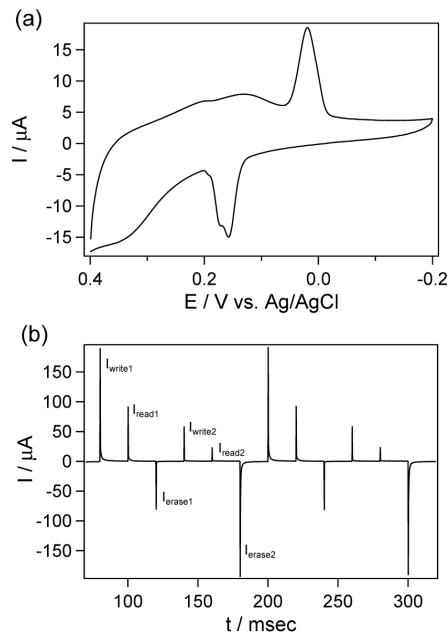


FIGURE 2.10

a) Cyclic voltammogram observed for cytochrome c and azurin hybrid layer onto the gold surface in 10 mM PBS (pH 7.0); b) Charging currents observed upon application of two different of input pulse potentials of oxidation ($I_{\text{write } 1,2}$), open-circuit ($I_{\text{read } 1,2}$), and reduction ($I_{\text{erase } 1,2}$) potentials were applied to gold electrodes having a pulse width of 20 ms for a total duration of 320 ms. Figure reproduced with permission from: ref. 22, © 2010 WILEY-VCH

Figure 2.10 (b) shows the faradaic currents obtained for a multi-level operation of a protein-based memory device. Faradaic currents were obtained when the heterolayer was applied with an oxidation potential of 0.324 V vs. Ag/AgCl and the cytochrome c layers became oxidized. Now the electrode was left open for a small duration of time and again when connecting the OCP of 0.104 V vs. Ag/AgCl large amplitude currents were monitored in the absence of background currents. When a reduction potential 0.131 V was applied, the stored charge was erased, this was evident by the small amplitude currents. In the same way, faradaic currents were obtained when an oxidation potential of 0.184 V vs. Ag/AgCl was applied to the heterolayer. Under these conditions, the recombinant azurin layers became oxidized, which was then reduced when a reduction potential of 0.062 V was applied to the recombinant azurin layer. After this, the electrode was left open for a small duration of time and again connecting the OCP of 0.150 V vs. Ag/AgCl resulted in the appearance of small amplitude currents in the absence of background currents. Here, applying 0.184 V was another writing step whereas applying 0.150 V was another reading step with respect to the measurement of currents. Finally, the application of 0.062 V erased the stored charge in the recombinant azurin layer. In this manner, two pairs of redox potentials were applied to the protein film for a duration of 320 ms, clear transient currents for the two pairs of the charge to *write*, *read*, and *erase* functions were monitored which are prerequisite for any molecular memory storage device.

Design of hybrid biomaterials

Ferritin a ubiquitous intracellular protein contains an iron metal ion (i.e., ferrihydrite core) conjugated with protein binding sites. By controlling the redox properties of the protein it was utilized as a memory storage element for charge trap/release of its $\text{Fe}^{\text{III}}/\text{Fe}^{\text{II}}$ redox center. Here, the single ferritin nanoparticle is about 12 nm size which was operated as a nanoscale-memory device and the layer by-layer assembled protein multilayer device had adjustable memory performance (Figure 2.11). Single protein as well as protein multilayers can be utilized as nanoscale memory device with non-volatile memory nature. Furthermore, it is demonstrated that the memory performance of protein multilayers can be significantly improved by layer-by-layer (LbL) multilayer design. Towards this, multilayer films composed of anionic ferritin and cationic poly-(allylamine hydrochloride) (PAH) were deposited onto Pt-coated substrates using the electrostatic LbL assembly method.

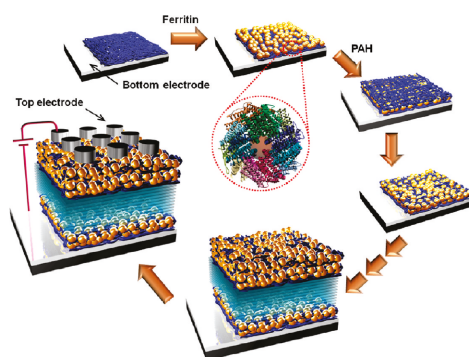


FIGURE 2.11

Schematics for the setup of PAH/ferritin multilayer-based nonvolatile memory devices. Figure reproduced with permission from: ref. 23, © 2011 ACS

The electrical measurements of nonvolatile memory cells were performed using applied voltage in an air atmosphere. In a typical bipolar switching measurement that depends on voltage polarity, voltage sweeps from -2.0 V to $+2.0$ V and back to -2.0 V were applied with the current limited to 100 mA. The high-current state (ON state) formed after the initial electroforming stage (for a conductive path within multilayers) was suddenly converted to a low-current state (RESET process for OFF state) at $+1.5$ V when the reverse voltage polarity was applied to the $(\text{PAH/ferritin})_{n=5,10,15}$ multilayered devices. This low-current state (OFF state) was maintained from $+2.0$ V to -1.5 V and then converted to the high-current state at -1.5 V (SET process for ON state). In addition, an increased number of bilayers (i.e., increased multilayer thickness) significantly lowered the OFF current level because the increased film thickness decreased the electric field level (Figure 2.12). As a result, the ON/OFF current ratio of these devices was increased to $\sim 10^3$.

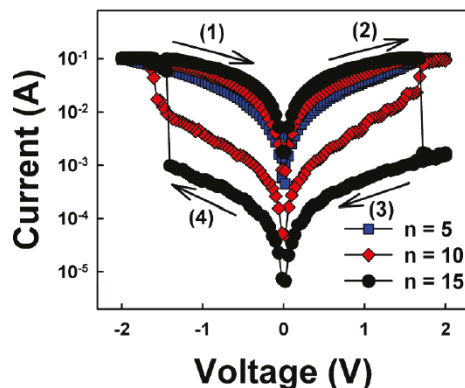


FIGURE 2.12

I-V curves of $(\text{PAH/ferritin})_n$ multilayer devices with bilayer number (n) from $n = 5$ to 15. Figure reproduced with permission from: ref. 23, © 2011 ACS

New concepts for advanced biomemory devices

With electronic devices becoming smaller every day, the field of molecular electronics has become ever more critical in solving the problem of further miniaturization, and single molecules represent the limit of miniaturization. Therefore, molecules have a typical size of a few nanometers, making them the ultimate limit for down-sizing present-day electronic components, such as diodes, transistors and memory devices. Hence, the continued advances in memory technology will require the development of nanoscale devices, of which the two terminal device architecture appears especially promising since the overall size of the device is dictated by the size of the electrodes [24]. Nonvolatile memory devices have been made by sandwiching electrically switchable materials (bistable materials, donor acceptor charge transfer complexes, nanocomposites constructed by bio/organic molecules coupled with nanoparticles) between the two electrodes [25]. By controlling the voltage between the two electrodes, the conductance of the materials is switched to different values to represent a memory device [26].

Nanostructured biomaterials represent an ideal system for use in bio-electronic devices (memory and sensors) for their unique size and properties. Important developments have been made in the synthesis of bio nanostructures with nanocrystals, including protein coupled with metallic and/or semiconducting nanoparticles [27]. Hence, hybrid structures containing inorganic nanoparticles have currently emerged as excellent candidates for potential applications in next generation nonvolatile memory devices [28]. Using these hybrid structures several non-volatile memory device has been proposed. Among the several types of nonvolatile memory devices, bistable devices have been particularly interesting and promising candidates for next-generation nonvolatile memory devices due to their relatively simple fabrication process without additional electrode contacts (sources and drain) [29].

Novel hybrid biomaterials higher storage density and information processing

Until now various protein and electrode structures to demonstrate various biomemory functions such as multilevel, multifunctional, 4-bit biomemory devices were discussed. To overcome this

limitation of molecular electronics, a new bioprocessing device was demonstrated that can perform various functions with a single hybrid molecule, derived from a biomemory device with a simple metalloprotein [30]. The suggested bioprocessing device has versatile functionality unavailable in current silicon-based electronic devices. Usually, organic molecular-based electronic devices operate with simple functions such as switching that require integration of various elements [31]. However, the present bioprocessing device mimics the modulating signals with various biochemical inputs that are associated with enzymatic or bio-catalytic reactions, which is similar to human brain organics such as “action-reaction” systems. Biochemical reactions can be observed as change in bulk material properties or structural re-organizations at the single-molecule level occurs. These reactions can be established in machine language, thus allowing to express all the chemical processes in terms of computing operations instead of traditional chemical material transformations. This concept could be extended to bio-hybrid molecular-based Biocomputing systems [32].

Figure 2.13 represents a bioprocessing device based on a single hybrid molecule that performs ‘information reinforcement,’ ‘information regulation,’ and ‘information amplification’ functions. These independent functions originate from the interaction between redox properties of metalloprotein and external input materials. To obtain three different functions on a single biohybrid material in the bioelectronic device, a recombinant azurin with deoxyribonucleic acid (DNA) (Azu/DNA) hybrid molecule using a chemical ligation method (CLM) was designed. Figure 2.13 (a) shows the basic concept of the memory modulating mechanism. This mechanism shows the interaction between the redox property of metalloprotein and the input materials. Figure 2.13 (b) shows the recombinant azurin utilized as a memory platform, where the DNA acts as a modulation operator. Also, figure 2.13 (c) shows gel electrophoresis results for the formation of protein-DNA hybrid system which can be utilized for various information processing when the modulation inputs (i) heavy metal ions, (ii) cDNA couple with Au nanoparticles and (iii) cDNA coupled to quantum dots are couple to the hybrid structure. The response to modulation input were performed with electrochemical measurements and the information amplification function using DNA-semiconducting nanoparticles as a modulation input was accomplished through scanning tunneling spectroscopy (STS) measurements.

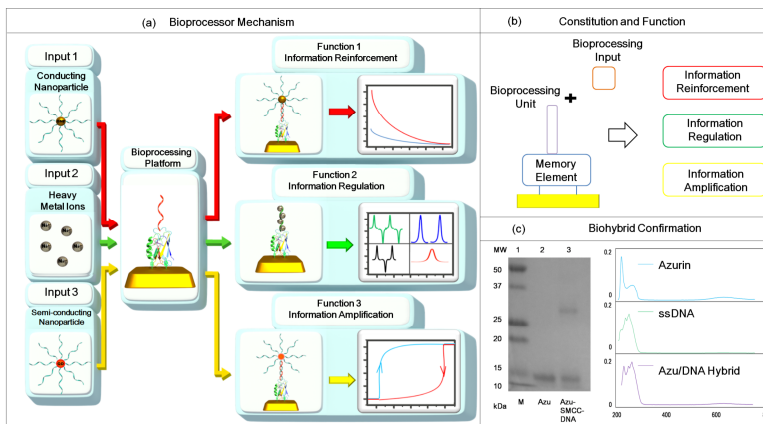


FIGURE 2.13

Schematic diagram of bioprocessing device. (a) Bioprocessing mechanism; (b) constitution and function and (c) shows gel electrophoresis results for the formation of protein-DNA hybrid system. Figure reproduced with permission from: ref. 33, © 2013 WILEY-VCH

Single molecular and solid state biomemory devices

Molecular-scale components are expected to be key in realization of nanoscale electronic devices. While molecular-scale switching has been reported in atomic quantum point contacts, single-molecule junctions with on/off conductance states with variety of molecularly tailored materials are also promising towards next generation memory devices. Further, switching in single-molecule junctions was achieved through the changes in conformation or charge state of the biomolecule. To achieve a single molecule based biomemory device for real world applications need to overcome many challenges and technical difficulties. Primarily, it is difficult to control the arrangement of each protein molecule on the solid substrate and to analyze its properties for application to an electronic device due to the fact that the size of a biomolecule is nanometer scale [34]. Yet again, the key function of such proteins is performed in the environment of a solution. Some hindrances caused by the surroundings, such as ions of the electrolyte and a distance effect, occur in the process of electron transfer because the electrical and electrochemical signals of the biomaterials pass through the solution. However, the conditions of high vacuum and extremely low temperature used in the studies of organic or inorganic materials could exclude the effects of surroundings. One solution to address this issue to develop nanoscale biomemory devices such as nano gap electrodes with single protein molecules which can be mass produced. Further, Electron transfer through individual molecules has been probed recently using electrochemical scanning tunneling microscopy (EC-STM) [35]. In EC-STM, a gate voltage is used to align a protein redox level to the Fermi levels of the tip and substrate with the sample in solution at room temperature. According to resonant tunneling models, electrons transfer via resonant tunneling due to alignment of molecular orbital energy levels with the Fermi level of the contact electrodes. In the two-step process, conformational changes in the molecule occur during tunneling which change the orbital energy levels. This process is thought to be especially prevalent in redox molecules [36].

Recently study describes a single-electron transistors composed of the myoglobin (Mb) a redox protein based nano gap electrode junction was demonstrated [37]. The nanogap junctions were fabricated from Pt thin films, 8-10 nm thick in the middle, 200 nm wide and deposited on a Si wafer with a 200 nm thick SiO₂ insulating layer. The doped Si substrate was used as a gate contact in all samples, as shown in figure 2.14. Electrical measurements were performed immediately after breaking the junction at low temperature (either 77 or 6 K). The conductance (dI/dV) as a function of V_b and V_G was acquired by numerically differentiating current–bias voltage (I – V) curves.

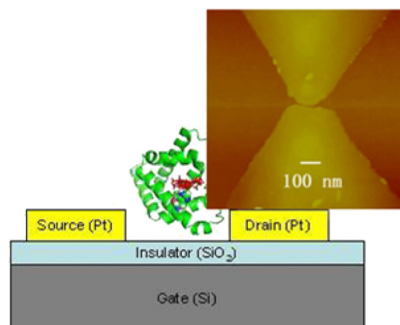


FIGURE 2.14

Sketch of a three-terminal device and AFM image of a bare Pt junction broken by electromigration. The AFM image indicate that the gap is on the order of 5 nm wide. Figure reproduced with permission from: ref. 37, © 2012 IOP Publishing Ltd

Figure 2.15 shows the results from one of the Mb in nanogap electrode sample which resulted a Kondo-like resonance. When the junction was initially broken by a negative electrical pulse, no conductance peaks were found. However, there was a sudden increase in the current when the voltage was increased again, indicating a modification of the contact and possible protein incorporation in the gap of electrodes, although this could also be due to Joule heating resulting from a sudden narrowing of the junction in the contact region. In the differential conductance map, with Mb between the nanogap as shown in figure 2.15(a), two intense peaks around $V_B = 0$ are independent of V_G for $0 < V_G < 3$ V. For higher V_G values, the peaks are composed of half a Coulomb-blockade-like triangle. This could be an indication of a Kondo-resonance assisted tunneling [38], although verification would require measurement in large magnetic fields. The two lines indicated by the green arrows, corresponding to the green arrows in figure 2.15(a), do not depend strongly on V_G for $0 < V_G < 1$ V. The conductance feature starting at $V_B \approx 30$ mV could arise from vibrational excitations as this energy coincides with the energy of the Fe-His vibration (27.3 meV). Conductance steps are also present as indicated in figure 2.15(b). These steps result in peaks in d^2I/dV^2 , indicated by the black (9 mV), blue (35 mV), and magenta (≈ 80 mV) arrows in figure 2.15(b). Taking into account that modes increase in energy at low T, the arrows correspond to heme-doming, Fe-His, and, heme group deformation (83.7 meV) modes, respectively.

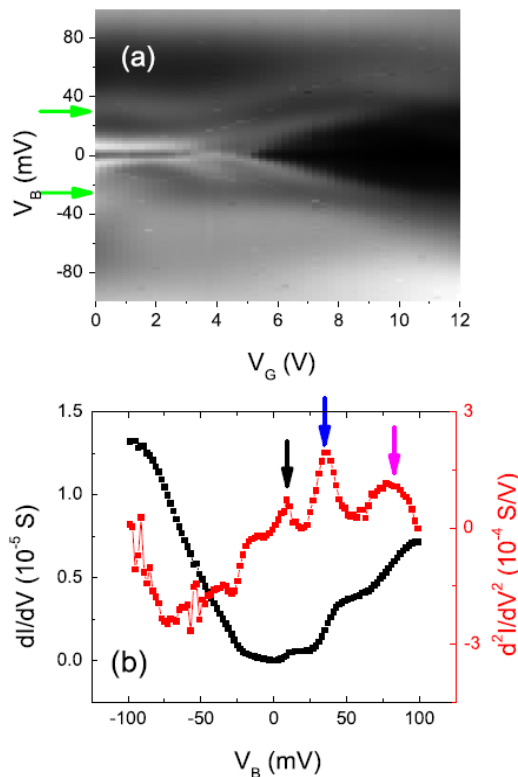


FIGURE 2.15

Mb results. (a) dI/dV as a function of V_B and V_G at $T = 6$ K (gray scale is 0 (black) to 1.33×10^{-5} S (white)). The green arrow point to conduction lines corresponding to Fe-His vibration-assisted tunneling. (b) dI/dV (black) and d^2I/dV^2 (red) spectra at $V_G = 1.1$ V. The vertical arrows correspond to inelastic tunneling peaks. Figure reproduced with permission from: ref. 37, © 2012 IOP Publishing Ltd

In another study, the advantages of single protein electrochemistry coupled with ECSTM as powerful tools to disclose the electronic structures and properties of a bacterial electron transfer protein, cytochrome b₅₆₂ (cyt b₅₆₂) was examined [39]. To facilitate direct self-assembly of cyt b₅₆₂ on a metal surface such as gold or platinum, the protein has been engineered to introduce a thiol-linking group via the amino acid cysteine on the protein surface. SDM was used to generate the cyt b₅₆₂ D50C variant (Figure 2.16a), in which aspartic acid (D) at position 50 was substituted with cysteine (C).

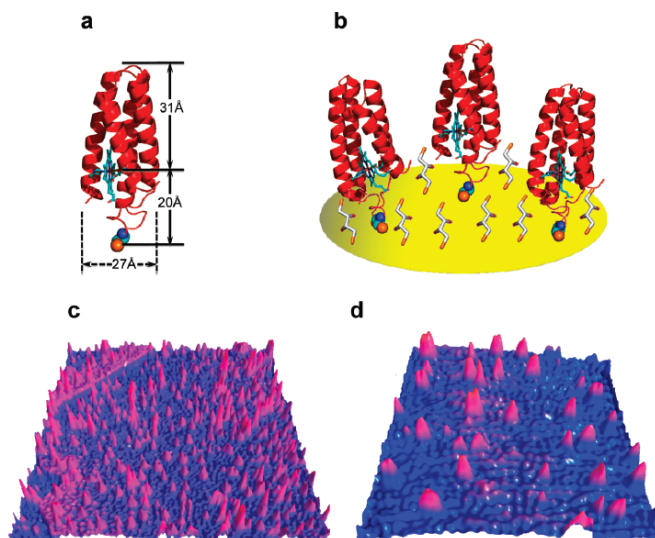
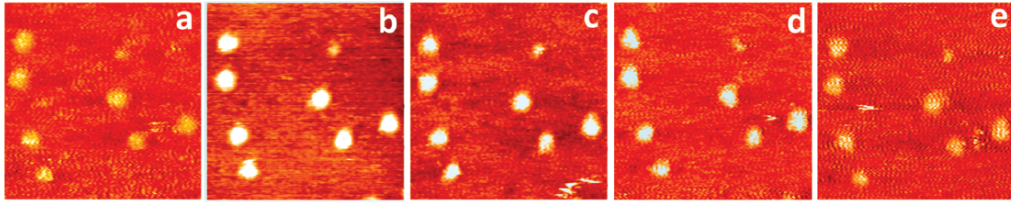


FIGURE 2.16

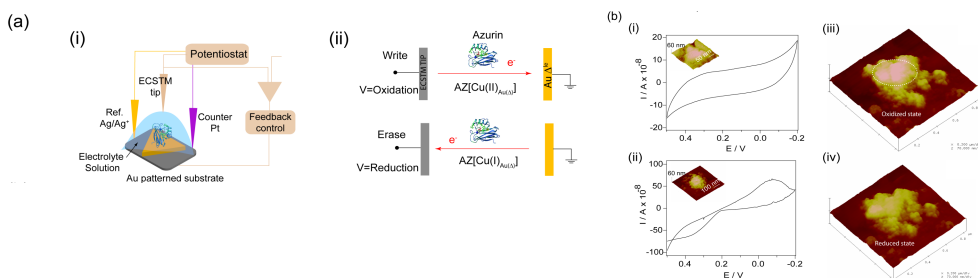
Three-dimensional structure and sizes of cyt b₅₆₂ D50C, (b) a schematic illustration of cyt b₅₆₂ D50C self-assembled, along with small molecules 1,4-dithiothreitol (DTT) on an Au(111) surface, and (c,d) three-dimensional STM images obtained in a phosphate buffer (10 mM, pH 6.2) under electrochemical control. The ECSTM imaging parameters: the tunneling current (I_t) 35 pA, bias voltage (V_b) -0.4 V, working electrode potential (E_w) -0.10 V vs SCE; image sizes (c) 150 nm \times 150 nm and (d) 90 nm \times 90 nm. Figure reproduced with permission from: ref. 39, © 2011 ACS

The mutation displayed a little effect on the redox properties of cyt b₅₆₂. Cyt b₅₆₂ D50C was observed to self-assemble on an Au (111) surface via thiol-gold chemistry to form a monolayer or sub-monolayer, depending on the protein concentration and adsorption time. To facilitate single-molecule measurements, 1,4-dithiothreitol (DTT) was co-adsorbed with the protein to yield a mixed monolayer (Figure 2.16b). Here DTT played two crucial roles: (1) to act as a reducing agent to prevent the formation of protein dimers in solution via disulfide bonds, and (2) to serve as a surface diluent to generate isolated protein molecules. Figure 2.16 (c,d) shows two three dimensional (3D) STM images with different scanned areas as examples. The image in Figure 2.16c was obtained from the samples prepared with relatively high protein population, while the low surface coverage (as shown in Figure 2.16(d)) is suitable for single-molecule measurements.

**FIGURE 2.17**

ECSTM images for direct visualization of single molecule protein electron transfer in cytochrome b562 D50C under different overpotentials (a) -250 , (b) -10 , (c) $+50$, (d) $+150$, (e) $+200$ mV. The bias voltage (V_b) = -0.4 V and tunneling current (I_t) = 35 pA. The image size is 32 nm \times 32 nm. Figure reproduced with permission from: ref. 39, © 2011 ACS

Electron transfer can also be investigated by electrochemical scanning tunneling microscopy (ECSTM) which shows that the apparent height of individually resolved redox proteins changes with the overpotential of the ECSTM electrodes, as a result of a redox gate effect on the protein tunneling conductance. This method enables to directly measure ET currents with individual redox proteins bridged between two electrodes. Direct visualization of single-molecule protein electron transfer by STM was conducted in the constant-current mode at a small tunneling current of 35 pA. STM imaging was first performed over a larger scan area such as 150×150 nm² to obtain images of the protein sub-monolayer at molecular resolution and then focused on a few individual molecules by gradually reducing the scan area. By keeping a constant bias voltage between the substrate and the tip, STM imaging started with the substrate potential set around the equilibrium redox potential of cyt b₅₆₂ D50C (i.e., zero overpotential, $\eta = E_w - E^{0\oplus}$). Imaging was continued toward either positive or negative overpotentials by adjusting the substrate and tip potentials in parallel (i.e., with fixed bias voltage) and finally returned to the equilibrium potential. As a result, a series of STM images at various overpotentials were acquired. Figure 2.17 shows some representative images focused on seven protein molecules. The single-molecule tunneling contrast is clearly tuned by the redox state of the protein, with a maximum contrast around the overpotential of -10 to -20 mV (Figure 2.17b), very close to the equilibrium redox potential. The contrast decreases upon applying either negative (Figure 2.17a) or positive (Figure 2.17c-e) overpotentials with the effects being quite symmetric. Therefore, high resolution ECSTM enables us to visualize redox-gated tunneling resonance at the single-molecule level.

**FIGURE 2.18**

(a) Schematic diagram shows (i) Az/Au triangle with ECSTM set-up and (ii) electron transfer mechanism in Az/Au nano-triangle during oxidation and reduction potentials. (b) CV's for (i) bare and (ii) AZ/Au/ITO in 10 mM buffer solution pH 7.0 at a scan rate of 50 mV/s. Inset show ECSTM image of (i) bare Au and (ii) AZ/Au/ITO surface. Potential dependent ECSTM images of AZ/Au/ITO for (iii) oxidation (0.36 V) and (iv) reduction potentials (-0.07) respectively. Figure reproduced with permission from: ref. 40, © 2013 WILEY-VCH

By using electrochemical scanning probe microscopy with in-situ cyclic voltammetry experiments memory function experiments were performed. To realize a practical biomemory device single detection system is not enough, to ensure the possibility of multiple detection systems to read the stored and erased charges states optical and magnetic detection systems were also incorporated [40].

Furthermore, nanoscale protein based memory device, in which the recombinant protein is self-assembled on Au pattern formed indium tin oxide (ITO) coated glass plate was also demonstrated. Electrochemical experiments on Az/Au-ITO were conducted by ECSTM with in-situ cyclic voltammetry. Experiments were carried out in 10mM HEPES buffer solution, where the Az/Au-ITO substrate acts as working electrode (vs. Ag/Ag⁺) as shown in Fig. 2.18a (i) along with the biomemory mechanism is shown in Fig. 2.18a (ii). The CV curves of bare Au nanopattern did not reveal any redox peaks; moreover, the CV for azurin on the Au nanopattern clearly depicted the peak reduction at -0.07 V and an oxidation peak at 0.36 V, respectively, at a scan rate of 50 mV/s, which corresponded to the redox process of the Cu^{2+/1+} center in azurin, as shown in Fig. 2.18b (i and ii). These two redox states of azurin were used for charge storage and erase functions to develop a molecular switch for the ON and OFF function. The stability of the two redox states was analyzed by applying many consecutive voltage cycles, which resulted in completely identical voltammogram's without any loss in current intensity. It was performed as a reversible and stable switch with an Az/Au-ITO electrode also from the imaging it was observed a change in conductance of the redox molecules upon varying the potential which was reflected in a difference in apparent height with respect to the background. Fig. 2.17b (iii and iv) shows the images for the applied potential of 0.36 and -0.07 V respectively for a bias voltage (V_B) of 100 mV for oxidation and reduction states of azurin molecules. The bright spots on the Au nanotriangles, which contained azurin, were attributed to electron tunneling enhancement due to the presence of the Cu active site. These morphological changes appeared to be strongly dependent on the redox potentials.

By using the Au pattern ITO as a reference electrode, it was observed that an intense peak (λ_{max}) appeared at 621 nm upon applying a voltage of $E = 0.36$ V. Additionally, applying $E = -0.07$ V resulted in an intense peak (λ_{max}) at 638 nm and a weaker peak at 510 nm. These peaks were due to the ligand-to-metal-charge transfer transition ($S(Cys - \pi) \rightarrow Cu(II) d_{x^2-y^2}$) involving the Cu atom of the active site and one of the five metal ligands (specifically, Cys 112) [41], which has a band gap energy of 1.98 eV with the ($S(Cys - \sigma) \rightarrow Cu(II) d_{x^2-y^2}$) transition [42], respectively. All these spectral changes are a clear indication of the transformation of Az and its redox states, and the process was reversible. It is known that reduced azurin has diamagnetic behavior and oxidized azurin behaves as paramagnetic [43]. Hence, magnetic output can also be used to perform the molecular switch for read-out mechanism of the switch. Thus, combined techniques such as electrochemical, optical and magnetic detection methods for oxidized and reduced forms of azurin can be exploited towards nanoscale biomemory device.

Conclusions

The discussed results back the conviction that proteins are interesting materials in developing nanoscale memory device. Not only for developing memory devices but also due to their structural and functional versatility, they are potentially suited to a wide range of applications. Further development toward commercial applications can be envisaged as (at least) tenfold.

On the edge of molecular electronics protein-based circuits can be conceived of as an interesting solution, once appropriate techniques for patterning and interconnecting devices are made available. The nanoscopic size of the computing units-down to a single molecule-and their possibly low cost can be the strengths of new molecular machines. Conversely, novel architectures and computing paradigms are necessary to meet the constraints of this novel bioelectronic components to realize for practical applications.

In the memory device operation, memory characteristics should be obtained without the operation of STM which demands the proper external connecting circuitry which is mandatory for developing a new generation nanoscale memory device. Also these molecules coupled to Au nano-scale pattern are of great interest and could be the possible candidate for the next generation memory devices. Using the self-assembly properties of proteins and possibly other molecules (e.g., DNA) can lead to very complex macroscopic structures, achieving finer-than-lithographic resolution without use of traditional lithography. This is, in fact, what is necessary to build memories and complex computing circuits. Therefore, these proteins based electronics could be a true beginning of the post-silicon era.

Acknowledgements

This research was supported by the National Research Foundation of Korea (NRF) grant funded by the Korea government (MSIP) (No. 2014R1A2A1A10051725) and Leading Foreign Research Institute Recruitment Program, through the National Research Foundation of Korea (NRF), funded by the Ministry of Science, ICT and Future Planning (MSIP) (2013K1A4A3055268).

References

1. W. G. Kuhr, Integration of Molecular Components into Silicon Memory Devices, *The Electrochemical Society Interface – Spring*, 34-38, 2004.
2. S.J. Kim, J. Jung, K. W. Lee, D. H. Yoon, T.S. Jung, S.R. Dungasani, S.H. Park, H.J. Kim, Low-Cost Label-Free Electrical Detection of Artificial DNA Nanostructures Using Solution-Processed Oxide Thin-Film Transistors, *ACS Appl. Mater. Interfaces*, 5 (21), 10715–10720, 2013.
3. J. Wang, Cargo-towing synthetic nanomachines: Towards active transport in microchip devices, *Lab Chip*, 12, 1944-1950, 2012.
4. T. Miyamoto, S. Razavi, R. DeRose, T. Inoue, Synthesizing Biomolecule-based Boolean Logic Gates. *ACS Synthetic Biology*, 2(2), 72-82, 2013.
5. K. T. Hamorsky, C. M. Ensor, Y. Wei, S. Daunert, A Bioluminescent Molecular Switch For Glucose, *Angew. Chem. Int. Ed.* 47, 1-4, 2008.
6. Y. Ogura, T. Beppu, M. Takinoue, A. Suyama, J. Tanida, Control of DNA Molecules on a Microscopic Bead Using Optical Techniques for Photonic DNA Memory, Springer-Verlag Berlin Heidelberg, A. Carbone and N.A. Pierce (Eds.): 213-223, 2006.
7. M. Pita, E. Katz, Multiple logic gates based on electrically wired surface-reconstituted enzymes, *J. Am. Chem. Soc.* 130, 36-37, 2008.

8. A. S. Deonarine, S. M. Clark, L. Konermann, Implementation of a multifunctional logic gate based on folding/unfolding transitions of a protein, *Future Generation Computer Systems* 19, 87-97, 2003.
9. A. Tinazli, J. Piehler, M. Beuttler, R. Guckenberger, R. Tampe, Native protein nanolithography that can write, read and erase, *Nature Nanotechnology* 2, 220-225, 2007.
10. W. G. Kuhr, A. R. Gallo, R. W. Manning, C. W. Rhodine, Molecular Memories Based on a CMOS Platform, *MRS Bulletin*, 29,11, 838-842, 2004.
11. M. Knez, U. Gosele, Bionanoelectronics: Viruses show their good side, *Nature Nanotechnology*, 1, 22-23, 2006.
12. J.-W. Choi, B.-K. Oh, Y. J. Kim, J. Min, Protein-based biomemory device consisting of the cysteine-modified azurin, *Appl. Phys. Lett.* 91, 263902 (2007).
13. C. Nicolini, From neural chip and engineered biomolecules to bioelectronic devices: An overview, *Biosens Bioelectron*, 1995, 10, 105-127.
14. G. Gilardi, A. Fantuzzi, Manipulating redox systems: application to nanotechnology, *Trends in Biotechnology*, 19,1,468-476.
15. T. Vo-Dinh, The new paradigm shift at the convergence of nanotechnology, molecular biology and biomedical sciences, *Nanobiotechnology* 1, 3-6, 2005.
16. A.K. Yagati, S.-U. Kim, J. Min, J.-W. Choi, Write-Once-Read-Many-Times (WORM) biomemory device consisting of cysteine modified ferredoxin, *Electrochem. Commun.*, 11, 854-858, 2009.
17. M. Jung, S. Lee, Y. T. Byun, Y. M. Jhona, S. H. Kim, D.-H. Woo, and S.-I. Mho, Characteristics and Fabrication of Nanohole Array on InP Semiconductor Substrate using Nanoporous Alumina, *Microelectronics Journal*, 39 526-528, 2008.
18. C. L. Haynes, R.P. Van Duyne, Nanosphere Lithography: A Versatile Nanofabrication Tool for Studies of Size-Dependent Nanoparticle Optics, *J. Phys. Chem. B*, 105, 5599-5611, 2001.
19. A.K. Yagati, T. Lee, J. Min, J.-W. Choi, A robust nanoscale biomemory device composed of recombinant azurin on hexagonally packed Au-nano array, *Biosens. & Bioelectron.* 40, 283-290, 2013.
20. A.K. Yagati, S.-U. Kim, J. Min, J.-W. Choi, Multi-bit biomemory consisting of recombinant protein variants, azurin, *Biosens. & Bioelectron.* 24, 1503-1507, 2009.
21. T. Lee, J. Min, S.-U. Kim, J.-W. Choi, Multifunctional 4-bit biomemory chip consisting of recombinant azurin variants, *Biomaterials* 32, 3815-3821, 2011.
22. T. Lee, S.-U. Kim, J. Min, J.-W. Choi, Multilevel Biomemory Device Consisting of Recombinant Azurin/Cytochrome c, *Adv. Mater.* 22, 510-514, 2010.
23. Y. Ko, Y. Kim, H. Baek, J. Cho, Electrically bistable properties of layer-by-layer assembled multilayers based on protein nanoparticles, *ACS NANO* 5, 9918-9926, 2011.
24. I. Salaoru, S. Paul, Memory devices based on small organic molecules donor-acceptor system, *Thin Solid Films*, 519, 559-562, 2010.
25. C.-W. Liu, C.-L. Cheng, K.-S. Chang-liao, J.-T. Jeng, B.-T. Dai, C.-P. Tsai, Characterization of TiOxNy nanoparticles embedded in HfOxNy as charge trapping nodes for nonvolatile memory device applications, *Microelectronic Engineering* 86, 1692-1695, 2009.
26. M. Novak, M. Burkhardt, A. Jedaa, M. Halik, Flexible copper-7,7,8,8 tetracyanochinodimethane memory devices-Operation, cross talk and bending, *Thin Solid Films* 518, 2222-2227, 2010.

27. S. Behrens, J. Wu, W. Habicht, F. Unger, Silver Nanoparticle and Nanowire Formation by Microtubule Templates, *Chem. Mater.*, **16**, 3085-3090, 2004.
28. W. L. Leong, P.S. Le, S.G. Mhaisklkar, T. P. Chen, A. Dodablapur, Charging phenomena in pentacene-gold nanoparticle memory device, *Appl. Phys. Lett.*, **90**, 042906-042908, 2007.
29. R. J. Warburton, C. Schaflein, D. Haft, F. Bickel, A. Lorke, K. Karrai, J. M. Garcia, W. Schoenfeld, P. M. Petroff, Optical emission from a charge-tunable quantum ring, *Nature (London)* **405**, 926-929, 2000.
30. G. Strack, M. Pita, M. Ornatska, E. Katz, Boolean Logic Gates that Use Enzymes as Input Signals, *Chem. Bio. Chem.* **9**, 1260-1266, 2008.
31. H. Gu, J. Chao, S.-J. Xiao, N. C. Seeman, A proximity-based programmable DNA nanoscale assembly line *Nature* **465**, 202-205, 2010.
32. M. Amrute-Nayak, R. P. Diensthuber, W. Steffen, D. Kathmann, F. K. Hartmann, R. Fedorov, C. Urbanke, D. J. Manstein, B. Brenner, G. Tsiavaliaris, Targeted Optimization of a Protein Nanomachine for Operation in Biohybrid Devices, *Angew. Chem. Int. Ed.*, **49**, 312-316, 2010.
33. T. Lee, A.K. Yagati, J. Min, J.-W. Choi, Bioprocessing Device Composed of Protein/DNA/Inorganic Material Hybrid, *Adv. Funct. Mater.*, **24**, 1781-1789, 2013.
34. C. Pedersen, H. Vallhov, H. Engqvist, A. Scheynius, M. Strømme, Nanoscale Size Control of Protein Aggregates, *Small*, **9**, 3320-3326, 2013.
35. Q. Chi, O. Farver, J. Ulstrup, Long-range protein electron transfer observed at the single-molecule level: *In situ* mapping of redox-gated tunneling resonance, *PNAS*, **102**, 16203-16208.
36. Q. Chi, J. Zhang, P. S. Jensen, H. E.M. Christensen, J. Ulstrup, Long-range interfacial electron transfer of metalloproteins based on molecular wiring assemblies, *Faraday Discuss.*, **131**, 181-195, 2006.
37. D. Li, P. M. Gannett, D. Lederman, An investigation into the feasibility of myoglobin-based single-electron transistors, *Nanotechnology* **23**, 395705 (10pp), (2012).
38. D. Goldhaber-Gordon, H. Shtrikman, D. Mahalu, D. Abusch-Magder, U. Meirav, M. A. Kastner, Kondo effect in a single-electron transistor, *Nature* **391**, 156-159, 1998.
39. E. A.D. Pia, Q. Chi, D. D. Jones, J. E. Macdonald, J. Ulstrup, M. Elliott, Single-Molecule Mapping of Long-range Electron Transport for a Cytochrome b562 Variant, *Nano Lett.*, **11**, 176-182, 2011.
40. A. K. Yagati, T. Lee, J. Min, J.-W. Choi, A robust nanoscale biomemory device composed of recombinant azurin on hexagonally packed Au-nano array, *Biosens. & Bioelectron.*, **40**, 283-290, 2013.
41. E. I. Solomon, J. W. Hare, D. M. Dooley, J. H. Dawson, P. J. Stephens, H. B. Gray, Spectroscopic studies of stellacyanin, plastocyanin, and azurin. Electronic structure of the blue copper sites, *J. Am. Chem. Soc.*, **102**, 168-178, 1980.
42. J. Han, T. M. Loehr, Y. Lu, J. S. Valentine, B. A. Averill, J. Sanders-Loehr, Resonance Raman excitation profiles indicate multiple Cys .fwdarw. Cu charge transfer transitions in type 1 copper proteins, *J. Am. Chem. Soc.*, **115**, 4256-4263, 1993.
43. C. M. Groeneveld, G.W. Canters, The pH dependence of the electron self-exchange rate of azurin from *Pseudomonas aeruginosa* as studied by ¹H-NMR. *European Journal of Biochemistry* **153**, 559-564, 1985.